ulation of vibrational states. The only requirements are the knowledge of the vibrational wave function and a vibrational cooling time that is shorter than the usable lifetime of the ions in a storage ring. Most heteronuclear molecular ions satisfy this criterion.

References and Notes

1. *Atomic and Molecular Beam Methods*, G. Scoles, Ed. (Oxford Univ. Press, New York, 1988).
2. T. G. Slanger, L. E. Jusinski, G. Black, G. E. Gadd, *Science* **241**, 945 (1988).
3. J. N. Bardsley and M. A. Biondi, *Adv. Mol. Phys.* **6**, 1 (1970).
4. D. Kella, L. Vejby-Christensen, P. J. Johnson, H. B. Pedersen, L. H. Andersen, *Science* **276**, 1530 (1997).
5. S. L. Guberman, *ibid.* **278**, 1276 (1997).
6. J. B. A. Mitchell, *Phys. Rep.* **186**, 215 (1990).
7. M. Larsson, *Annu. Rev. Phys. Chem.* **48**, 151 (1997), and references therein.
8. P. Forck *et al.*, *Phys. Rev. Lett.* **72**, 2002 (1994).
9. J. R. Mowat *et al.*, *ibid.* **74**, 50 (1995).
10. Z. Amitay *et al.*, *Phys. Rev. A* **54**, 4032 (1996).
11. C. Strömholm *et al.*, *ibid.* **52**, 4320 (1995).
12. Z. Vager, R. Naaman, E. P. Kanter, *Science* **244**, 426 (1989).
13. D. Zajfman and Z. Amitay, *Phys. Rev. A* **52**, 839 (1995).
14. D. Habs *et al.*, *Nucl. Instrum. Methods* **B43**, 390 (1989).
15. D. Zajfman, T. Graber, E. P. Kanter, Z. Vager, *Phys. Rev. A* **46**, 194 (1992).
16. M. Tadjeddine and G. Parlant, *Mol. Phys.* **33**, 1797 (1977).
17. Z. Amitay, D. Zajfman, P. Forck, *Phys. Rev. A* **50**, 2304 (1994).
18. H. Takagi, in *Dissociative Recombination: Theory, Experiment and Applications III*, D. Zajfman, J. B. A. Mitchell, D. Schwalm, B. R. Rowe, Eds. (World Scientific, Singapore, 1996), pp. 174–183.
19. K. Nakashima, H. Takagi, H. Nakamura, *J. Chem. Phys.* **86**, 726 (1987).
20. A. Giusti-Suzor, *J. Phys. B* **13**, 3687 (1980); S. Guberman and A. Giusti-Suzor, *J. Chem. Phys.* **95**, 2602 (1991).

21. Supported in part by the German Federal Minister for Education, Science, Research and Technology under contract number 06 HD 854I, by the Human Capital and Mobility Programme of the European Community, and by the German Israel Foundation under contract number I-0452-200.07/95.

3 March 1998; accepted 13 May 1998

An Inverted Hexagonal Phase of Cationic Liposome–DNA Complexes Related to DNA Release and Delivery

Ilya Koltover, Tim Salditt,* Joachim O. Rädler,† Cyrus R. Safinya‡

A two-dimensional columnar phase in mixtures of DNA complexed with cationic liposomes has been found in the lipid composition regime known to be significantly more efficient at transfecting mammalian cells in culture compared to the lamellar (L_α^C) structure of cationic liposome–DNA complexes. The structure, derived from synchrotron x-ray diffraction, consists of DNA coated by cationic lipid monolayers and arranged on a two-dimensional hexagonal lattice (H_{II}^C). Two membrane-altering pathways induce the $L_\alpha^C \rightarrow H_{II}^C$ transition: one where the spontaneous curvature of the lipid monolayer is driven negative, and another where the membrane bending rigidity is lowered with a new class of helper-lipids. Optical microscopy revealed that the L_α^C complexes bind stably to anionic vesicles (models of cellular membranes), whereas the more transfectant H_{II}^C complexes are unstable and rapidly fuse and release DNA upon adhering to anionic vesicles.

Complexes consisting of DNA mixed with oppositely charged cationic liposomes (CLs; closed bilayer membrane shells of lipid molecules) mimic natural viruses in their ability to act as synthetic carriers of extracellular DNA across outer cell membranes and nuclear membranes for gene delivery (*1–3*). The use of nonviral rather than viral methods for gene delivery has several advantages, including nonimmunicity and the potential for transferring and expressing (transfecting) large pieces of DNA into cells. Partial sections of first-generation human artificial chromosomes (HACs) on the order of 1 Mbp can be transferred into cells by means of CLs, although extremely inefficiently (*4*). The low transfection efficiencies of nonviral delivery methods may be improved through insights into transfection-related mechanisms at the molecular and self-assembled levels.

The efficiency of transfection mediated by mixtures of cationic lipids and so-called neutral "helper-lipids" varies widely and unpredictably (*1, 3, 5*). The choice of the helper-lipid has been empirically established to be important; for example, transfection of mammalian cells in culture is efficient in mixtures of the univalent cationic lipid DOTAP (dioleoyl trimethylammonium propane) and the neutral helper-lipid DOPE (dioleoyl phosphatidylethanolamine), and not in mixtures of DOTAP and a similar helper-lipid, DOPC (dioleoyl phosphatidylcholine) (*6*). We recently showed that mixing DNA with CLs consisting of DOPC and DOTAP leads to a topological transition into condensed CL-DNA complexes with a multilamellar structure (L_α^C), with DNA monolayers sandwiched between cationic lipid bilayers (*7*) in a manner similar to the schematic in Fig. 1 (left).

Using synchrotron small-angle x-ray scattering (SAXS) and optical microscopy, we found a completely different columnar inverted hexagonal H_{II}^C liquid-crystalline state in CL-DNA complexes (Fig. 1, right). The commonly used helper-lipid DOPE induces the $L_\alpha^C \rightarrow H_{II}^C$ structural transition by controlling the spontaneous curvature $C_o = 1/R_o$ of the lipid monolayer, where R_o is the natural radius of curvature (Fig. 1, pathway I). We also identified a class of helper molecules that control the membrane bending rigidity κ and give rise to a second pathway to the H_{II}^C phase (Fig. 1, pathway II). The CL-DNA complexes containing DOPE that are empirically known to transfect exhibit the H_{II}^C phase, rather than the L_α^C structure found in complexes containing DOPC. Optical imaging showed that complex interactions with model cell membranes mimicking the early stages of transfection are structure-dependent.

Synchrotron SAXS scans of positively charged CL-DNA complexes for $\rho = 3$ are shown in Fig. 2A as a function of increasing Φ_{DOPE} in the DOPE-DOTAP CL mixtures along pathway I (*8*). [Here and below, ρ denotes the DOTAP/DNA weight ratio, Φ_{DOPE} is the weight fraction DOPE/(DOPE + DOTAP), and Φ_{DOPC} is the weight fraction DOPC/(DOPC + DOTAP).] The complexes are charged positively for $\rho > 2.2$ and negatively for $\rho < 2.2$, which indicates that charge reversal occurs when complexes are stoichiometrically neutral (with one positive lipid per negatively charged nucleotide base). At $\Phi_{DOPE} = 0.41$, SAXS scans of the lamellar L_α^C complex (Fig.

Materials Department, Physics Department, and Biochemistry and Molecular Biology Program, University of California, Santa Barbara, CA 93106, USA.

*Present address: Sektion Physik der Ludwig-Maximilians-Universität München, Geschwister-Scholl-Platz 1, 80539 München, Germany.

†Present address: Physikdepartment, Technische Universität München, Institut für Biophysik (E22), James Franck-Strasse, 85747 Garching, Germany.

‡To whom correspondence should be addressed.

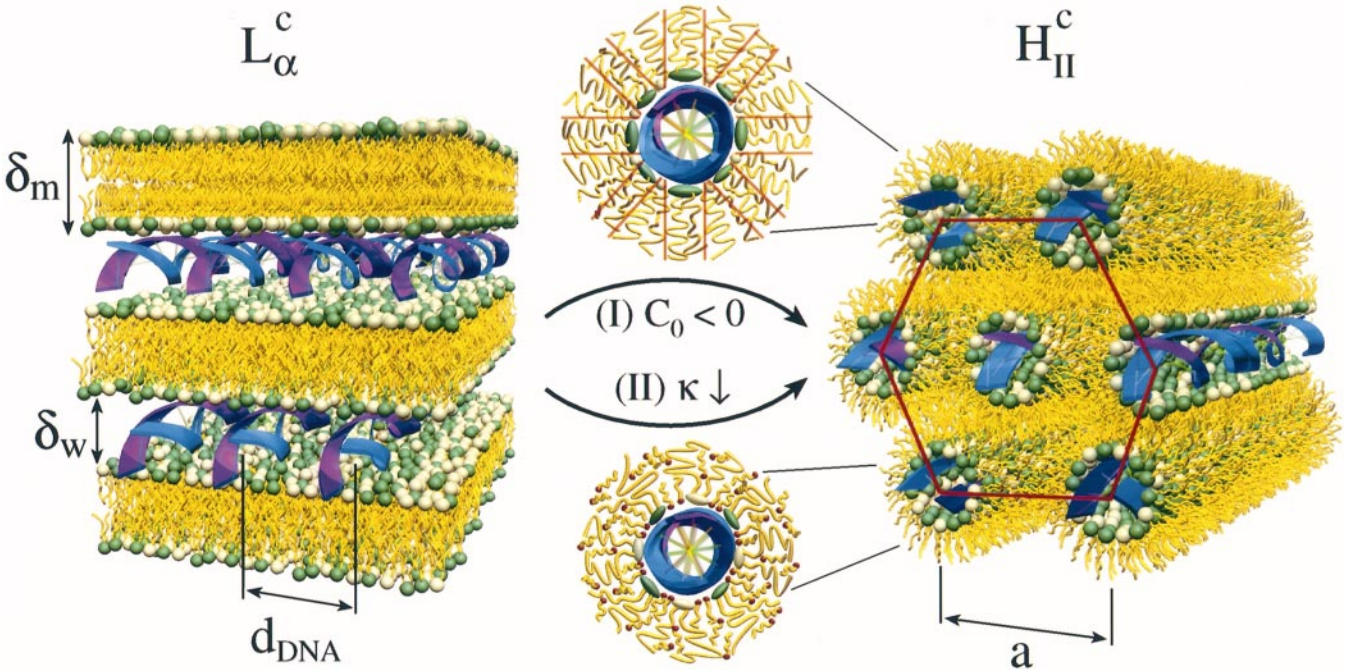

Fig. 1. Schematic of two distinct pathways from the lamellar L_α^C phase to the columnar inverted hexagonal H_{II}^C phase of CL-DNA complexes. Along pathway I, the natural curvature $C_o = 1/R_o$ of the cationic lipid monolayer is driven negative by the addition of the helper-lipid DOPE. This is shown schematically (center top); the cationic lipid DOTAP is cylindrically shaped whereas DOPE is conelike, leading to the negative curvature. Along pathway II, the $L_\alpha^C \rightarrow H_{II}^C$ transition is induced by the addition of helper-lipids consisting of mixtures of DOPC and the cosurfactant hexanol, which reduces the membrane bending rigidity.

2A) show sharp peaks at $q_{001} = 0.099$ Å^{-1} and $q_{002} = 0.198$ Å^{-1} from the lamellar periodic structure ($d = 2\pi/q_{001} = 63.47$ Å) with DNA intercalated between cationic lipid bilayers (Fig. 1, left). Because the DOPE-DOTAP bilayer thickness at $\Phi_{DOPE} = 0.41$ is $\delta_m = 40$ Å (*9*), the water gap between bilayers $\delta_w = d - \delta_m = 23.47$ Å is just large enough to accommodate a hydrated monolayer of DNA. The middle broad peak at $q_{DNA} = 0.172$ Å^{-1} is due to the one-dimensional (1D) array of DNA chains, with the spacing between the DNA strands $d_{DNA} = 2\pi/q_{DNA}$. This structure, found in CL-DNA complexes with $\Phi_{DOPE} < 0.41$, is analogous to that reported recently (*7*, *10*).

For $0.7 < \Phi_{DOPE} < 0.85$, the peaks of the SAXS scans of the CL-DNA complexes are indexed perfectly on a 2D hexagonal lattice with a unit cell spacing of $a = 4\pi/[(3)^{0.5}q_{10}] = 67.4$ Å for $\Phi_{DOPE} = 0.75$. We observed Bragg peaks up to the seventh order, which indicates a high degree of regularity of the structure. At $\Phi_{DOPE} = 0.75$, the first- through fourth-order Bragg peaks of this hexagonal structure occur at $q_{10} = 0.107$ Å^{-1}, $q_{11} = 0.185$ Å^{-1}, $q_{20} = 0.214$ Å^{-1}, and $q_{21} = 0.283$ Å^{-1} (Fig. 2A). This is consistent with a 2D columnar inverted hexagonal structure (Fig. 1, right), which we refer to as the H_{II}^C phase of CL-DNA complexes. The DNA molecules are surrounded by a lipid monolayer, with the DNA-lipid inverted cylindrical micelles arranged on a hexagonal lattice. The structure resembles that of the inverted hexagonal H_{II} phase of pure DOPE in excess water (*11*), with the water space inside the lipid micelle filled by DNA. The greater electron density of DNA with respect to water leads to the relative suppression of the (11) and (20) Bragg peak intensities compared with

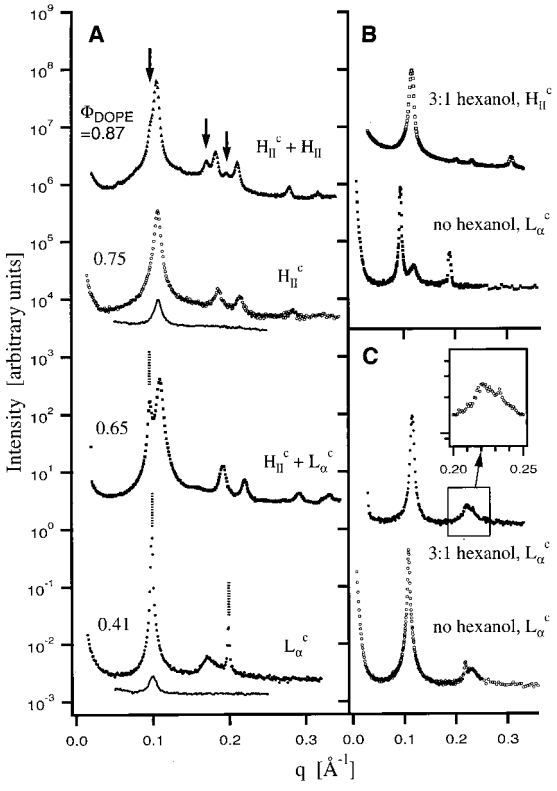

Fig. 2. Synchrotron SAXS patterns of the lamellar L_α^C and columnar inverted hexagonal H_{II}^C phases of positively charged CL-DNA complexes. (**A**) SAXS scans of CL-DNA complexes as a function of increasing Φ_{DOPE} along pathway I of Fig. 1. At $\Phi_{DOPE} = 0.41$, the SAXS pattern results from a single phase with the L_α^C structure shown in Fig. 1 (left). At $\Phi_{DOPE} = 0.75$, the SAXS scan results from a single phase with the H_{II}^C structure shown in Fig. 1 (right). At $\Phi_{DOPE} = 0.65$, the SAXS shows coexistence of the L_α^C (dotted line) and H_{II}^C phases. At $\Phi_{DOPE} = 0.87$, SAXS shows coexistence of the H_{II}^C phase and the inverted hexagonal H_{II} phase of pure DOPE (arrows). SAXS patterns of complexes made from extremely dilute DNA (0.01 mg/ml) and lipid (0.1 mg/ml) solutions are plotted as solid lines for $\Phi_{DOPE} = 0.41$ and 0.75. (**B**) SAXS scans of CL-DNA at a constant Φ_{DOPC} with no hexanol (a cosurfactant) and at a hexanol/total lipid molar ratio of 3:1 along pathway II of Fig. 1. With no hexanol (filled squares), the structure is lamellar L_α^C, whereas the complexes with hexanol (open squares) exhibit the hexagonal H_{II}^C structure. (**C**) SAXS scans of CL-DNA complexes with $\Phi_{DOPC} = 0$. The complexes remain in the L_α^C phase with and without added hexanol.

that in the lipid H_{II} phase (*9*). If we assume an average lipid monolayer thickness of 20 Å, the diameter of the micellar void in the H_{II}^C phase is near 28 Å, again sufficient for a DNA molecule with approximately two hydration shells. For $0.41 < \Phi_{DOPE} < 0.7$, the L_α^C and H_{II}^C structures coexist as shown at $\Phi_{DOPE} = 0.65$ and are nearly epitaxially matched with $a \approx d$. For $\Phi_{DOPE} > 0.85$, the H_{II}^C phase coexists with the H_{II} phase of pure DOPE, which has peaks at $q_{10} = 0.0975$ Å^{-1}, $q_{11} = 0.169$ Å^{-1}, and $q_{20} = 0.195$ Å^{-1} (arrows in Fig. 2A at $\Phi_{DOPE} = 0.87$) with a unit cell spacing of $a = 74.41$ Å.

SAXS scans of CL-DNA complexes at the concentration (0.01%) typically used in cell transfection studies (*6*) are also plotted in Fig. 2A (solid lines at $\Phi_{DOPE} = 0.41$ and 0.75). The complexes have their first-order Bragg peaks at exactly the same positions as in the corresponding more concentrated (1%) samples. Thus, the internal structures of the complexes are independent of the overall DNA and lipid concentrations.

The $L_\alpha^C \rightarrow H_{II}^C$ phase transition can be induced along a second pathway (Fig. 1, pathway II) with a new type of helper-lipid mixture. Complexes containing mixtures of DOPC and DOTAP exhibited the lamellar L_α^C structure (*7*), as shown by the SAXS scan in Fig. 2B (bottom; $\Phi_{DOPC} = 0.7$) with an interlayer spacing of $d = 2\pi/q_{001} = 66.84$ Å. As a function of increasing ratio of hexanol (a membrane-soluble cosurfactant) to DOPC, we found a structural transition to the H_{II}^C phase. The first four SAXS peaks for complexes containing DOPC, DOTAP, and hexanol ($\Phi_{DOPC} = 0.7$; hexanol/total lipid molar ratio, 3:1) can be indexed on a hexagonal lattice with a unit cell size $a = 62.54$ Å. In CL-DNA complexes of pure DOTAP (Fig. 2C), hexanol addition did not induce the transition and we always found the L_α^C structure. In this case, the only effect of the addition of hexanol is to thin the cationic bilayer membrane (consisting of hexanol:DOTAP at a 3:1 molar ratio) from $d = 57.91$ Å to 54.17 Å. The interaxial DNA-DNA spacing d_{DNA} was also observed to increase from 27.1 to 28.82 Å, consistent with a decrease in the membrane charge density with the addition of hexanol.

To understand the $L_\alpha^C \rightarrow H_{II}^C$ transition qualitatively along the two pathways in Fig. 1, we consider the interplay between the electrostatic and membrane elastic interactions in the complexes. Pure electrostatic interactions alone are expected to favor the H_{II}^C phase, which minimizes the charge separation between the anionic groups on the DNA chain and the cationic lipids (*1, 12*). The electrostatic interaction may be resisted by the Helfrich elastic cost (per unit area) of forming a cylindrical monolayer membrane around DNA

$$F/A = 0.5\kappa(1/R - 1/R_o)^2 \qquad (1)$$

where κ is the lipid monolayer rigidity, R is the radius of curvature, and R_o is the natural radius of curvature. Along pathway I (Fig. 1), cationic DOTAP with $1/R_o^{DOTAP} = 0$ favors the flat lamellar L_α phase, but DOPE has a negative natural curvature $1/R_o^{DOPE} < 0$; that is, DOPE has a larger area per two chains than area per head group (Fig. 1, center top) and forms the inverted hexagonal H_{II} phase (*11*). Thus, along pathway I, as a function of increasing Φ_{DOPE} (with $1/R_o = \Phi_{DOPE}^V/R_o^{DOPE}$, where Φ_{DOPE}^V is the volume fraction of DOPE), we expect a transition to the H_{II}^C phase because the membrane elastic energy favors a curved interface (Fig. 2A).

Along pathway II, the membrane bending rigidity κ is reduced significantly because of the addition of the membrane-soluble cosurfactant molecule hexanol. Cosurfactant molecules cannot stabilize an interface separating hydrophobic and hydrophilic regions, but when mixed with longer chain "true" surfactants they can lead to large changes in interface elasticities. The addition of hexanol to membranes of lamellar phases with a molar ratio of 2 to 4 will lead to a decrease of κ from $\sim 20\ k_BT$ (where k_BT is the thermal energy) to between 2 and 5 k_BT (*13*). Simple compressional models of surfactant chains show that κ scales with chain length l_n ($\propto \delta_m$, membrane thickness; n = number of carbons per chain) and the area per lipid chain A_L as $\kappa \propto l_n^3/A_L^5$ (*14*), and hexanol both decreases l_n and increases A_L (*13, 14*) (Fig. 1, center bottom). The addition of cosurfactant results in a reduction in κ, and hence a reduction in the elastic energy barrier to the formation of the H_{II}^C phase favored by the electrostatic interactions. The transition to the H_{II}^C phase along pathway II occurs only in CL-DNA complexes with low enough charge density, where DOTAP/DOPC < 0.5 (*9*). In this regime where the L_α^C structure is retained in complexes with pure DOTAP with and without added hexanol (Fig. 2C), the SAXS data are consistent with theory, which predicts a renormalized increase in κ with increasing surface charge density (*15*).

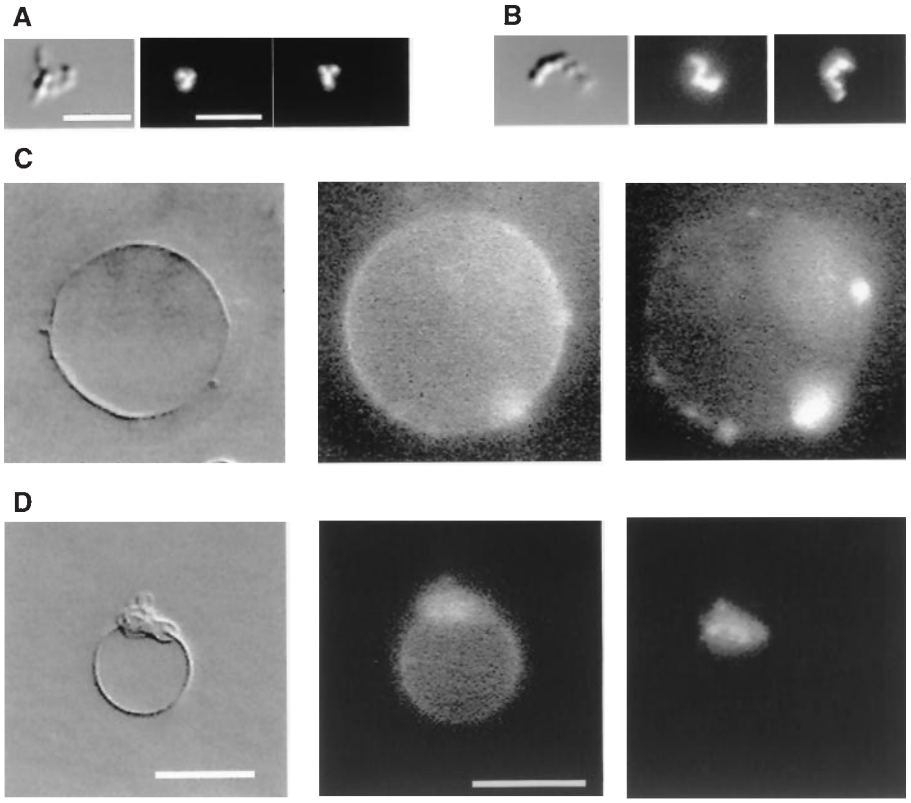

Fig. 3. Video microscopy images of positively charged CL-DNA complexes in the (**A**) H_{II}^C and (**B**) L_α^C phases, and interacting with negatively charged G-vesicles (**C** and **D**). In all cases, complexes were viewed by DIC (left), lipid fluorescence (middle), and DNA fluorescence (right). In (C) the L_α^C complexes simply stick to the G-vesicle and remain stable for many hours, retaining their bloblike morphology. The blobs are localized in DIC as well as in both fluorescence modes. In (D), the H_{II}^C complexes break up and spread immediately after attaching to G-vesicles, indicating a fusion process between the complex and the vesicle lipid bilayer. The loss of the compact structure of the complex is evident in both fluorescence modes. Scale bar for DIC images: 3 μm (A and B), 20 μm (C and D). Scale bar for fluorescence images: 6 μm (A and B)], 20 μm (C and D).

In the absence of DNA, mixtures of DOPC and DOTAP studied in this work with or without hexanol formed stable lamellar L_α phases (with $1/R_o = 0$) with no tendency to form the inverted H_{II} phase (*9*). However, DOPE-DOTAP-water mixtures formed coexisting H_{II} and L_α phases.

In both condensed phases, the complexes appear as highly dynamic birefringent aggregates when viewed with video-enhanced optical microscopy in differential interference contrast (DIC) and fluorescence configurations, as shown in Fig. 3A for H_{II}^C ($\Phi_{DOPE} = 0.73$) and Fig. 3B for L_α^C ($\Phi_{DOPE} = 0.3$) complexes along pathway I (*16*). The positive complexes (with $\rho = 3$) formed aggregates of connected blobs; with increasing complex charge, the aggregates became smaller and eventually dissociated into individual blobs. The L_α^C phase formed linear structures, whereas the H_{II}^C phase formed predominantly branched aggregates, which indicated that the shape of H_{II}^C complexes is inherently anisotropic (*9*). The observed overlap of lipid and DNA distributions in the two fluorescence modes (Fig. 3, A and B) shows that the complexes are highly compact objects with a close association of lipid and DNA.

To understand the effect of structure on the early stages of transfection, we studied the interaction of CL-DNA complexes with giant anionic vesicles (G-vesicles), which are models of cellular membranes (for example, plasma membrane; anionic endosomal vesicles). The main entry route to mammalian cells is believed to be endocytosis, where a local inward deformation of the cell plasma membrane leads to budding off of an internal vesicle forming the early-stage endosome (*17*). Thus, at the early stages of cell transfection, an intact CL-DNA complex may be captured inside an anionic endosomal vesicle.

The positively charged H_{II}^C and L_α^C complexes interacted very differently with model anionic lipid membranes, even when both types of structures contained DOPE. Typical micrographs of positively charged ($\rho = 4$) complexes immediately after mixing with G-vesicles are shown in Fig. 3, C and D. L_α^C complexes attached to the fluid membranes of the G-vesicles and remained stable (Fig. 3C); no fusion occurred between the complex and the G-vesicle. L_α^C complexes containing DOPC (*7*) showed the same behavior. H_{II}^C complexes attached to the G-vesicle and rapidly fused with it, spreading and losing their compact structure (Fig. 3D, left). Because the amount of lipid in the complex was comparable with that in the G-vesicle and the fusion occurred rapidly, this produced multiple free lipid lamellae. The loss of the compact complex structure and the subsequent desorption of DNA molecules from membrane and their Brownian motion between the lamellae were seen in fluorescence images (Fig. 3D, center and left). This behavior is expected after fusion, which results in the mixing of cationic lipid (from the H_{II}^C complex) with anionic lipid (from the G-vesicle), effectively "turning off" the electrostatic interactions (which gave rise to the compact CL-DNA complexes) and releasing DNA molecules inside the space between the lamellae and the G-vesicle bilayer. Because the geometry is the inverse of that of CL-DNA complexes inside anionic endosomal vesicles, we expect that upon fusion DNA should be released and expelled outside the endosome within the cytoplasm (*18*). On longer time scales (a few hours), we observed lipid transfer between the L_α^C complexes and G-vesicles (*9*). Thus, the observation that DOPE-DOTAP L_α^C and DOPC-DOTAP L_α^C complexes do not fuse with G-vesicles reveals a kinetic rather than equilibrium effect. In principle, it may be possible to design L_α^C complexes with a lower kinetic barrier to fusion. Moreover, the reported behavior of complexes containing univalent cationic lipids may be different from that of multivalent cationic lipids.

Our findings correlate the self-assembled structure of CL-DNA complexes and transfection efficiency: The empirically established transfectant complexes containing DOPE in mammalian cell cultures exhibit the H_{II}^C structure rather than the L_α^C structure found in complexes containing DOPC (*7*). We have also found the H_{II}^C phase in two other negatively charged polyelectrolytes: polyglutamic acid (PGA), a model polypeptide, and polythymine (poly-T), a model of single-stranded oligonucleotides used in antisense delivery applications (*19, 20*). Optical microscopy reveals a likely reason for why the different structures transfect cells with varying efficiency: In contrast to L_α^C complexes, H_{II}^C complexes fused and released DNA when in contact with anionic vesicles, which are cell-free models of cellular membranes, in particular, anionic endosomal vesicles.

References and Notes

1. P. L. Felgner, *Sci. Am.* **276**, 102 (June 1997).
2. T. Friedmann, *ibid.*, p. 96; P. L. Felgner and G. Rhodes, *Nature* **349**, 351 (1991); J.-P. Behr, *Bioconjugate Chem.* **5**, 382 (1994); N. Zhu, D. Liggitt, Y. Liu, R. Debs, *Science* **261**, 209 (1993).
3. J.-S. Remy, C. Sirlin, P. Vierling, J.-P. Behr, *Bioconjugate Chem.* **5**, 647 (1994).
4. J. J. Harrington, G. VanBokkelen, R. W. Mays, K. Gustashaw, H. F. Willard, *Nature Genet.* **15**, 21994 (1997); W. Roush, *Science* **276**, 38 (1997).
5. J. Felgner *et al*., *J. Biol. Chem.* **269**, 2550 (1994).
6. H. Farhood, N. Serbina, L. Huang, *Biochim. Biophys. Acta* **1235**, 289 (1995); S. W. Hui *et al*., *Biophys. J.* **71**, 590 (1996).
7. J. O. Rädler, I. Koltover, T. Salditt, C. R. Safinya, *Science* **275**, 810 (1997).
8. The SAXS experiments were carried out at the Stanford Synchrotron Radiation Laboratory at 8 keV. CL-DNA complexes were prepared by mixing deionized water solutions of highly purified linear λ-phage DNA (5 mg/ml, 48502 bp; contour length of 16.5 μm) and cationic liposomes of mixed lipids (25 mg/ml) directly in a quartz x-ray capillary (diameter 1.5 mm) with $\rho = 3$, which yielded positive complexes. The CLs consisting of binary DOPE-DOTAP mixtures have an average size of 0.06 μm. During CL-DNA complex formation, cationic lipids replace DNA counterions, releasing the Na^+ and Cl^- ions into solution with a large entropic free energy gain (on the order of k_BT per released counterion). The result is a close association between DNA and lipid in a compact complex with an average size of 0.2 μm (*7*).
9. I. Koltover, T. Salditt, C. R. Safinya, unpublished data.
10. T. Salditt, I. Koltover, J. O. Rädler, C. R. Safinya, *Phys. Rev. Lett.* **79**, 2582 (1997).
11. J. M. Seddon, *Biochim. Biophys. Acta* **1031**, 1 (1989); S. M. Gruner, *J. Phys. Chem.* **93**, 7562 (1989).
12. S. May and A. Ben-Shaul, *Biophys. J.* **73**, 2427 (1997); N. Dan, *Biochim. Biophys. Acta* **1369**, 34 (1998).
13. C. R. Safinya, E. B. Sirota, D. Roux, G. S. Smith, *Phys. Rev. Lett.* **62**, 1134 (1989).
14. I. Szleifer, D. Kramer, A. Ben-Shaul, D. Roux, W. M. Gelbart, *ibid.* **60**, 1966 (1988).
15. G. D. Guttman and D. Andelman, *J. Phys. II (Paris)* **3**, 1411 (1993).
16. For fluorescence experiments, cationic lipids were labeled with 0.2 mol % of DHPE–Texas Red and DNA was labeled with YoYo-1 iodide at a ratio of 1 dye molecule per 15 bp. Complexes were prepared by gently mixing DNA (0.01 mg/ml) and lipid (0.1 mg/ml) stock solutions to yield $\rho = 3$ (*8*). The complexes were further diluted with deionized water for observation. Giant unilamellar vesicles were prepared from mixtures of 90% DOPC (neutral) and 10% dioleoyl phosphatidylglycerol (DOPG) (negatively charged) lipids.
17. J. Zabner, A. J. Fasbender, T. Moninger, K. A. Poelinger, M. J. Welsh, *J. Biol. Chem.* **270**, 18997 (1995); I. Wrobel and D. Collins, *Biochim. Biophys. Acta* **1235**, 296 (1995); J. Y. Legendre and F. C. Szoka, *Pharm. Res.* **9**, 1235 (1992); A. Lin, N. Slack, C. George, C. Samuel, C. R. Safinya, unpublished data.
18. Although fluorescence microscopy studies in mouse fibroblast cell cultures show more complex behavior overall, they also show some similar features (A. Lin, N. Slack, C. R. Safinya, unpublished data).
19. M.-Y. Chiang *et al*., *J. Biol. Chem.* **266**, 18162 (1991); K. Lappalainen *et al*., *Biochim. Biophys. Acta* **1196**, 201 (1994).
20. The phase diagram of CL-polyelectrolyte complexes is plotted in a supplementary figure available at www.sciencemag.org/feature/data/980994.shl showing the variation of the unit-cell parameters in the L_α^C and H_{II}^C complexes as a function of Φ_{DOPE} for DNA, a 100-bp poly-T, and PGA. The phase sequence ($L_\alpha^C \rightarrow L_\alpha^C + H_{II}^C \rightarrow H_{II}^C \rightarrow H_{II}^C + HII$) occurs at $\Phi_{DOPE} = 0.48$, 0.67, and 0.85 for λ-DNA; 0.65 and 0.8 for poly-T; and 0.6, 0.76, and 0.8 for PGA. The phase transition $L_\alpha \rightarrow L_\alpha + H_{II}$ occurs at $\Phi_{DOPE} = 0.3$ in DOPE-DOTAP mixtures without a polyelectrolyte. In pure lipids, the H_{II} phase is present only in coexistence with the L_α phase, which indicates that the polyelectrolytes stabilize the H_{II}^C phase. The observed different phase boundaries most likely originate from differences in diameter and linear charge density between the polyelectrolytes, which in turn leads to different required amounts of lipid monolayer bending around the polyelectrolyte in the H_{II}^C complex.

21. We thank R. Bruinsma, A. Ben-Shaul, J. Israelachvili, P. Pincus, W. Gelbart, T. Lubensky, and N. Dan for discussions. Supported by grants from the UC-Biotechnology Research and Education Program (97-02), NSF (DMR-9624091), Petroleum Research Foundation (31352-AC7), and Los Alamos National Laboratory (STB/UC:96-108). T.S. and J.O.R. acknowledge a Nato postdoctoral scholarship distributed by the DAAD and a DFG (Ra 655/1-1). The Materials Research Laboratory at Santa Barbara is supported by NSF grant DMR-9632716. The Stanford Synchrotron Radiation Laboratory is supported by the U.S. Department of Energy.

26 February 1998; accepted 18 May 1998